MTLA 27 (2023) 101700

Contents lists available at ScienceDirect

Materialia

journal homepage: www.elsevier.com/locate/mtla

Innovative transdermal drug delivery system based on amoxicillin-loaded gelatin methacryloyl microneedles obtained by 3D printing

Huseyin Erkus [a,b], Tuba Bedir [a,c], Elif Kaya [d], Gulgun Bosgelmez Tinaz [d], Oguzhan Gunduz [a,c,e], Mariana-Carmen Chifiriuc [f,g], Cem Bulent Ustundag [b,e,*]

[a] Center for Nanotechnology and Biomaterials Application and Research (NBUAM), Marmara University, Istanbul 34722, Turkey
[b] Department of Bioengineering, Faculty of Chemical and Metallurgical Engineering, Yildiz Technical University, Istanbul 34220, Turkey
[c] Department of Metallurgical and Materials Engineering, Faculty of Technology, Marmara University, Istanbul 34722, Turkey
[d] Department of Basic Pharmaceutical Sciences, Faculty of Pharmacy, Marmara University, Istanbul 34668, Turkey
[e] Health Biotechnology Joint Research and Application Center of Excellence, Istanbul 34220, Turkey
[f] Faculty of Biology, University of Bucharest, Bucharest 050095, Romania
[g] Romanian Academy of Sciences, Bucharest 010071, Romania

ARTICLE INFO

Keywords:
Gelatin methacryloyl
Hydrogel
Amoxicillin
Microneedle
DLP 3D printing
Transdermal drug delivery

ABSTRACT

The microneedle (MN) technology platform has a significant potential for enhancing the efficacy of transdermal drug delivery, by using micron-scale arrays with restricted geometries that pierce the skin non-invasively. In this paper, we developed gelatin methacryloyl (GelMA) MNs containing amoxicillin (AMX) as a novel transdermal delivery system using digital light processing (DLP) based 3D printing technology. With the DLP approach, MNs were obtained with high resolution and minimal lead times without geometric limitations. The 3D-printed AMX-loaded GelMA MNs were examined for their morphological, mechanical, swelling and antimicrobial properties as well as the drug release profile. The morphological analysis demonstrated the successful fabrication of the MNs with regular structure and sharp tips. The fabricated MNs displayed good mechanical properties consistent with 0.1 N/needle without breaking. Moreover, the results of the *in vitro* antibacterial activity assays indicated that AMX-loaded GelMA MNs have significantly inhibited the *Staphylococcus aureus* and *Escherichia coli* growth. These findings suggest that the 3D-printed drug-loaded GelMA MNs are a useful platform for transdermal therapeutic delivery and can be developed as a next-generation medical device for managing bacterial infections.

1. Introduction

Despite the multiple advantages of transdermal drug delivery which provides an improved bioavailability of the drug delivered into the body through the skin, better patient compliance, controlled drug release, minimal gastric mucosal irritation, and inhibition of first-pass metabolism [1–6], the biggest challenge is the rigid and non-permeable structure of the stratum corneum (SC), restricting the passage of the substance through the skin [5,7,8]. Only low molecular weight lipophilic drugs are allowed to pass through the SC layer [2,7]. Various transdermal drug delivery strategies such as ultrasound, iontophoresis, electroporation, various nanocarrier-loaded creams, and transdermal patches have been investigated to overcome this issue [6,10]. However, the limitations of these strategies have fostered the exploration of novel improvements. Microneedles (MNs) consisting of micron-sized needles in arrays represent a promising approach for the development of transdermal drug delivery systems that could overcome the rigid structure of the SC layer [5,9,10]. Due to their small size, the MNs pierce the skin painlessly and non-invasively, avoiding contact with dermal nerves and blood vessels, thereby increasing skin permeability, with minimum potential risks of skin injury and contamination [8,11–13]. Moreover, MNs allow small drug molecules, macromolecules (peptides, proteins, vaccines, nucleic acids etc.) and nanoparticles to pass through the SC layer and reach directly the systemic circulation [6,8]. In addition to these properties, cost-effectiveness, high patient compliance and efficient storage conditions are other outstanding properties [7,13].

Different types of materials have been used for the MNs manufacturing, including glass, silicon, metal, polymer and ceramics [10,14]. Considering their biocompatibility, biodegradability and drug-loading capacity as critical factors, polymeric MNs represent an

* Corresponding author at: Department of Bioengineering, Faculty of Chemical and Metallurgical Engineering, Yildiz Technical University, Istanbul 34220, Turkey.
E-mail address: cbustun@yildiz.edu.tr (C.B. Ustundag).

https://doi.org/10.1016/j.mtla.2023.101700
Received 30 October 2022; Accepted 27 January 2023
Available online 30 January 2023

attractive lead, having also convenient processability and low cost [15,16]. Hydrogel MNs are structured in cross-linked polymeric networks with high pore structure and biocompatibility, capable of absorbing water and biological fluids [7,17]. The MNs hydrophilic structure allows them to swell upon contact with the skin and to release the loaded drug into the epidermis or dermis [18]. Apart from these, hydrogel MNs have some superior properties compared to other types of MNs such as higher drug release capacity and controllable drug release rate by changing the cross-linking ratio [6,10]. Moreover, MNs can be sterilized before use and be easily removed from the skin without damaging either the MNs or the skin [19].

The materials used in the fabrication of hydrogel MNs must be non-toxic, biocompatible, biodegradable and capable of releasing drugs [10,17]. Hydrogels are simply divided into two classes according to their material structure: (1) natural hydrogels (gelatin, cellulose, alginate, chitosan, hyaluronic acid etc.) and (2) synthetic hydrogels (acrylate polymers, polylactide, polyvinyl alcohol and polyvinylpyrrolidone etc.) [20]. Synthetic polymers are superior to natural polymers in terms of mechanical performance [2]. On the other hand, natural polymers show better biocompatibility and biodegradability over synthetic polymers [2,10]. Gelatin is a protein-based polymer, which is derived from collagen through various processes and has the feature of promoting cell growth [21]. The presence of peptide groups such as arginine-glycine-aspartic acid (RGD) in its structure allows it to mimic the extracellular matrix (ECM) in terms of cell adhesion and protease degradation [22]. However, the mechanical properties of MNs obtained from pure gelatin are insufficient to puncture the SC and to provide a long-term drug release profile due to its rapid degradability [2]. Therefore, modified gelatin can be used instead of pure gelatin to fabricate MNs for drug delivery applications.

Gelatin methacryloyl (GelMA) with higher mechanical strength is obtained by modifying the amino groups in gelatin with methacrylate groups [23]. Since the structure of RGD peptide groups of gelatin does not change, GelMA also preserves the cell attachment and protease degradation sites [20,22]. Also, GelMA still shows good biodegradability and biocompatibility and has negligible immunogenicity [19]. Moreover, GelMA can be biologically functionalized by encapsulation of different molecules such as drugs, growth factors and cytokines [2,20]. In addition to these features, the drug release profile can be changed by changing the degree of methacrylation and crosslinking ratio. GelMA prepared by grafting methacrylic anhydride onto gelatin exhibits excellent photo-curability and can be crosslinked by ultraviolet (UV) or visible light in the presence of a photoinitiator [20,24].

Different microfabrication techniques such as micro-moulding, etching, and photolithography have been developed to fabricate MNs [23,25,26]. The size and shape of the MNs influence the penetration ability, drug loading capacity and release rates; however current approaches can fabricate MNs with limited geometries. Moreover, these techniques are complex and require multiple steps, long lead times and expensive equipment [27]. 3D printing is an additive manufacturing technique that offers advantages such as ease of use, cost-effectiveness and printing complex geometry structures compared to other MN fabrication techniques [17,28]. Digital Light Processing (DLP) is a photopolymerization-based 3D printing method. In this method, the cross-section of the model is projected onto the surface of the liquid photopolymer through the digital micromirror element, thus the irradiated photopolymer solidifies layer by layer [29]. Compared with the other methods, DLP is less affected by oxygen inhibition [30]. Besides, DLP enables higher resolution and faster printing than other 3D printing methods [13,30]. In addition, no additional process such as UV and heat treatment after printing is required after the DLP printing is used. Furthermore, any photo-curable material can be used for fabrication in this technique [17,31]. Owing to these advantages, DLP 3D printing is widely used in biomedical applications, to print complex structures such as to form vascular networks and neural channels [32], and therefore to obtain human organ models [33]. It is also used to obtain drug delivery systems such as the antitumoral compound dacarbazine [34,35], and biosensors [36]. One study used the DLP technique to fabricate MNs with various geometries for wound healing applications, followed by pulsed laser deposition of silver and zinc oxide thin films. This light-based technology has proven useful in the production of antimicrobial MN patches [37]. To the best of our knowledge, the DLP 3D printing approach has not been used before in the fabrication of drug-loaded GelMA MNs.

Antibiotics are widely used in the treatment of bacterial infections and are most commonly administered via oral or parenteral routes, being accompanied by many undesired side effects such as toxicity or dysbiosis. Antibiotic administration via GelMA MNs rather than the oral or parenteral routes can improve their bioavailability in a painless and minimally invasive manner. In this study, we developed antibiotic (amoxicillin-AMX) loaded GelMA MNs as a trandermal drug delivery system using the DLP 3D printing technique. The morphology, mechanical behaviours, and swelling abilities of 3D-printed AMX-loaded GelMA MNs were evaluated. Moreover, the drug release profile and antimicrobial properties of fabricated AMX-loaded MNs were studied *in vitro*.

2. Materials and Methods

2.1. Materials

Gelatin type A from porcine skin, methacrylic anhydride (MAA), lithium phenyl-2,4,6-trimethyl-benzoyl phosphinate (LAP), amoxicillin, and dialysis membrane (cut-off value 14 kDa and average flat width 43 mm) were obtained from Sigma–Aldrich (Darmstadt, Germany). Sodium carbonate, sodium hydroxide, hydrochloric acid fuming 37%, and Parafilm® M were purchased from Merck KGaA (Darmstadt, Germany). Phosphate-buffered saline (PBS, pH 7.4) was bought from ChemBio (Turkey). Sodium hydrogen carbonate (>99.7%) was purchased from ISOLAB (Eschau, Germany).

2.2. GelMA synthesis

GelMA was synthesized according to a previously described protocol [38]. Briefly, to obtain 10% (w/v) gelatin solution, 10 g of type A gelatin was dissolved in 100 mL carbonate bicarbonate buffer (CB) (0.1 M CB buffer including 3.18 g sodium carbonate and 5.86 g sodium bicarbonate in 1 L distilled water, pH 9) under constant stirring at 60 °C. Then, for each gram of gelatin, 0.1 mL of methacrylic anhydride (MAA) was added to the gelatin solution and the solution was stirred at 50°C for 3 hours, and then the pH was readjusted to 7.4 to stop the reaction. Next, the solution was dialyzed against distilled water at 37 °C for 5 days using a 14 kDa molecular-weight-cutoff (MWCO) membrane. After being dialyzed, lyophilized and the samples were stored at +4 °C until further use.

2.3. Design and DLP printing of GelMA MNs

Computer-aided design (CAD) files for MNs were developed using SolidWorks 2020. MNs were designed conical shaped with 650 μm height and 400 μm base width. MN arrays consisted of 6×6 needles on a 10×10×1 mm substrate. The software of the 3D printer, Chitubox, was used to slice the MN designs (Fig. 1A). MNs were fabricated using a commercially accessible DLP 3D printer (Phrozen Sonic Mini 8K, Phrozen Tech Co Ltd., Hsinchu, Taiwan) with a 12 mW/cm^2 light intensity and 405 nm light wavelength. The exposure time to UV light during the printing of MNs was set to 80 s.

To prepare a 6% (w/v) GelMA solution, the appropriate amount of GelMA was added to the PBS (pH = 7.4) and dissolved at 40 °C. For drug-loaded GelMA MNs, 0.5% (w/v) amoxicillin was added to the GelMA solution and stirred at room temperature until the drug was completely dissolved. Next, a photoinitiator (LAP) was added at a concentration of 0.5% (w/v) to both the blank GelMA and drug-loaded GelMA solutions

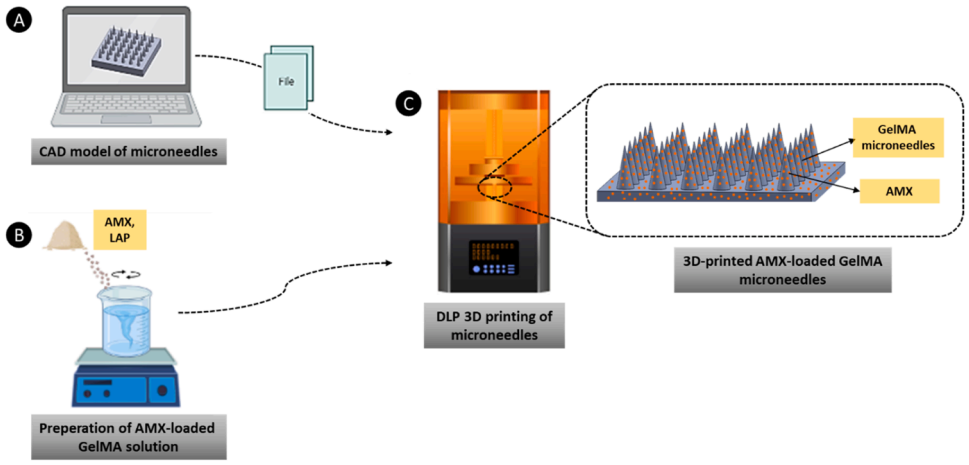

Fig. 1. Schematic illustration of the design and DLP 3D printing of AMX-loaded GelMA MNs.

and mixed until a homogeneous mixture was obtained (Fig. 1B). The prepared solution was discharged into the vat of the DLP printer. MNs were printed by the DLP device according to the parameters given above. One MN array was obtained per print and the time taken to print one MN array was 3.5 h. Then, 3D-printed MNs were dried at room temperature for 24 h and kept in a dehumidified container until characterization (Fig. 1C).

2.4. Morphological Characterization of GelMA MNs

The surface morphology of the GelMA MNs and AMX-loaded GelMA MNs were examined using a scanning electron microscope (EVA MA 10, Zeiss, Jena, Germany). Dried MNs were coated with gold using a spray coating machine (SC7620, Quorum, Laughton, East Sussex, UK) for 120 sec.

2.5. Fourier Transform Infrared Spectroscopy (FTIR)

Fourier transform infrared spectroscopy (FTIR, FT/IR-ATR 4700, Jasco, Easton, MD, USA) was used to determine the chemical structure of AMX, GelMA MNs and AMX-loaded GelMA MNs. The measurements were carried out at room temperature wavelength range of 450–4000 cm^{-1} at 4 cm^{-1} resolution.

2.6. Mechanical characterization and penetration test of GelMA MNs

The mechanical strength of MNs was measured by a standard mechanical tester (EZ-LX, Shimadzu, Kyoto, Japan) in compression mode. The MNs were placed on the flat surface of a stainless-steel base plate. The testing probe was positioned at 2 mm above the bottom of the MNs. An axial force was applied perpendicular to the axis of the MNs, at a constant speed of 0.1 mm/min. The resistance force as a function of MN base displacement was recorded by a moving sensor contacting the tip of the MN. All tests were performed in triplicate.

Studies in the literature have shown that Parafilm M® layers and pigskin have similar properties for penetration tests [39]. For this study, the penetration abilities of MNs were evaluated using Parafilm® M. The film, one layer of which was about 127 μm, was folded into 8 layers of approximately 1 mm. A thick layer of Parafilm M® was placed on a hard metal surface. The produced dry MNs were placed on top of the Parafilm M® layer with the needles coinciding with the Parafilm M®. The pressure was applied to the MNs with the help of the thumb. The MNs were then removed from the Parafilm M® layer. Parafilm M® layers were separated one by one and the number of holes and the hole width in each layer were evaluated using an optical microscope (Olympus AnalySIS, USA).

2.7. Swelling of GelMA MNs

To evaluate the swelling abilities of the GelMA MNs and AMX-loaded GelMA MNs, samples were immersed in PBS (pH = 7.4) at 37 °C for 30 min at specific time intervals (1, 5, 10, 15, 20, and 30 min). After the specified durations, the residual liquids on the surface were removed and the weights were recorded. The swelling ratio was calculated using the following Eq. (1):

$$Swelling\ ratio\ (\%) = \frac{Ww - W_d}{W_d} \times 100 \quad (1)$$

where W_d is the dry weight, and W_w is the weight of the MNs after water uptake at specified time intervals. All experiments were performed in triplicate.

2.8. In vitro drug release study

The release profile of AMX from MNs was investigated by measuring the UV–vis absorption of the drug in PBS (pH = 7.4) at predetermined time intervals. The standard curve of AMX was analyzed firstly by a UV–vis absorption spectrophotometer (Jenway 7315, Bibby Scientific, Staffordshire, UK) at a wavelength of 201 nm. The samples were kept at 37 °C in 1 mL of PBS. At predetermined time points, samples were taken out of the PBS solution, the amount of drug released was measured and the samples were placed into a fresh buffer solution to continue the release studies.

2.9. In vitro antimicrobial activity

The antibacterial activities of AMX-loaded GelMA MNs against *Staphylococcus aureus* (S. aureus) ATCC 25923 and *Escherichia coli* (*E. coli*) 25922 were tested using the disc diffusion method as described by the Clinical Laboratory Standards Institute (CLSI). Overnight cultures of S. aureus ATCC 25923 and *E. coli* 25922 with standard density corresponding to 0.5 MacFarland were spread onto Mueller-Hinton Agar plates, and then AMX-loaded GelMA MNs cut into 6 mm discs were placed on the agar plates and incubated at 37 °C for 24 h. The antibacterial activity was evaluated by measuring the growth inhibition zone diameters.

3. Results and Discussion

3.1. Morphological Characterization

GelMA MNs and AMX-loaded GelMA MNs were successfully fabricated by the DLP 3D printing technique with 80 s of UV exposure. SEM

images of the fabricated MNs are presented in Fig. 2. All MNs consisted of 6×6 needles on a 10×10×1 mm substrate by maintaining a conical shape. As shown in Fig. 2, the obtained MNs displayed regular morphology with sharp tips and no air bubbles or agglomerates in the structure. SEM images also confirmed the dimensions of the MNs: blank and AMX-loaded GelMA MNs were 630.4 ± 2 μm (Fig. 2A) and 621.5 ± 1 μm (Fig. 2B) in height, respectively. These heights are ideal for penetrating the skin barrier and preventing the skin-wrapping effect [40]. The obtained needle heights are lower than the theoretical needle height (650 μm). The height difference can be related to how a layer is drawn and the minimum UV dose necessary for photopolymerization. Normally, the light that each micromirror reflects spreads into adjacent pixels. Thereof, large pieces (where light from adjacent pixels comes together) have more amount of light per unit area than small pieces. Consequently, it is frequently difficult to cure small features. MN truncation is expected to occur when the width of the structure is reduced enough for the light intensity to fall below the minimum threshold for curing [27]. Tip radii of blank and AMX-loaded GelMA MNs were measured as 13.1 ± 2 μm and 15.9 ± 1 μm, respectively. The tip radii of 20–40 μm are sharp enough to penetrate the skin [41]. In this regard, the resulting tip radii are among the sharpest needles printed using a low-cost DLP printing system.

3.2. Fourier Transform Infrared Spectroscopy (FTIR)

The FTIR spectra of AMX, GelMA MNs and AMX-loaded GelMA MNs are displayed in Fig. 3. The spectrum of AMX exhibits peaks at around 3446 cm^{-1} and 2967 cm^{-1} representing the stretching vibrations of free amino groups and -CH, $-CH_2$ and CH_3 groups in AMX, respectively [42,43]. The peak at about 1683 cm^{-1} is attributed to the Amide I bond, the peak at about 1573 cm^{-1} to the Amide II bond, and the peak at about 1245 cm^{-1} to the Amide III bond [44,45]. 1625, 1523, 1444, 1396, 1336, 1240, and 1024 cm^{-1} peaks were obtained as a result of FTIR analysis of GelMA MNs. The sharp peak at around 1625 cm^{-1} showed the vibration of the C=O bonds known as Amide I [46]. The peak at about 1523 cm^{-1} is attributed to the N–H bonds known as Amide II. The vibrations peak observed at around 1240 cm^{-1} is related to the N–H bond (also part of the C–N bond), designated as Amide III [47]. Also, the peak observed in the range of 3200–3400 cm^{-1} is due to the presence of

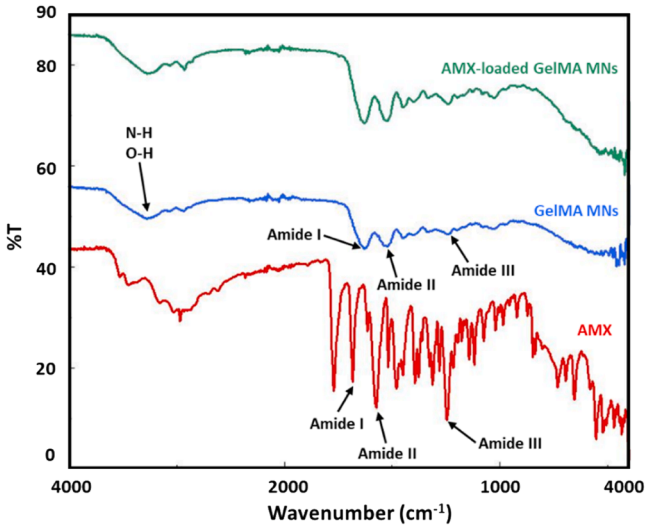

Fig. 3. FTIR spectra of AMX, GelMA MNs and AMX-loaded GelMA MNs.

peptide bonds (N–H stretching) and –OH functional groups [48]. There is no major change in the spectrum of AMX-GelMA MNs compared to the spectrum of GelMA MNs. Only slight shifts are observed in the position of the GelMA peaks. Since the amount of AMX in the MN structure is very low and therefore the FTIR technique remains insensitive, peaks of AMX could not be seen in the GelMA-AMX spectra.

3.3. Mechanical characterization and penetration test of GelMA MNs

The mechanical properties of MNs are a crucial factor affecting their capability of successfully penetrating the skin and delivering the drug efficiently into the skin [49,50]. The mechanical performance of GelMA MNs and AMX-loaded GelMA MNs was analyzed by a compression test. As can be seen in Fig. 4A, in the force-displacement curves, there was no discontinuity at 300 μm displacement, and no fracture or breakage was observed. This suggests that the fabricated MNs have convenient toughness. The maximum force determined at 300 μm displacement was 2.6 and 3.0 N for GelMA MNs and AMX-loaded GelMA MNs,

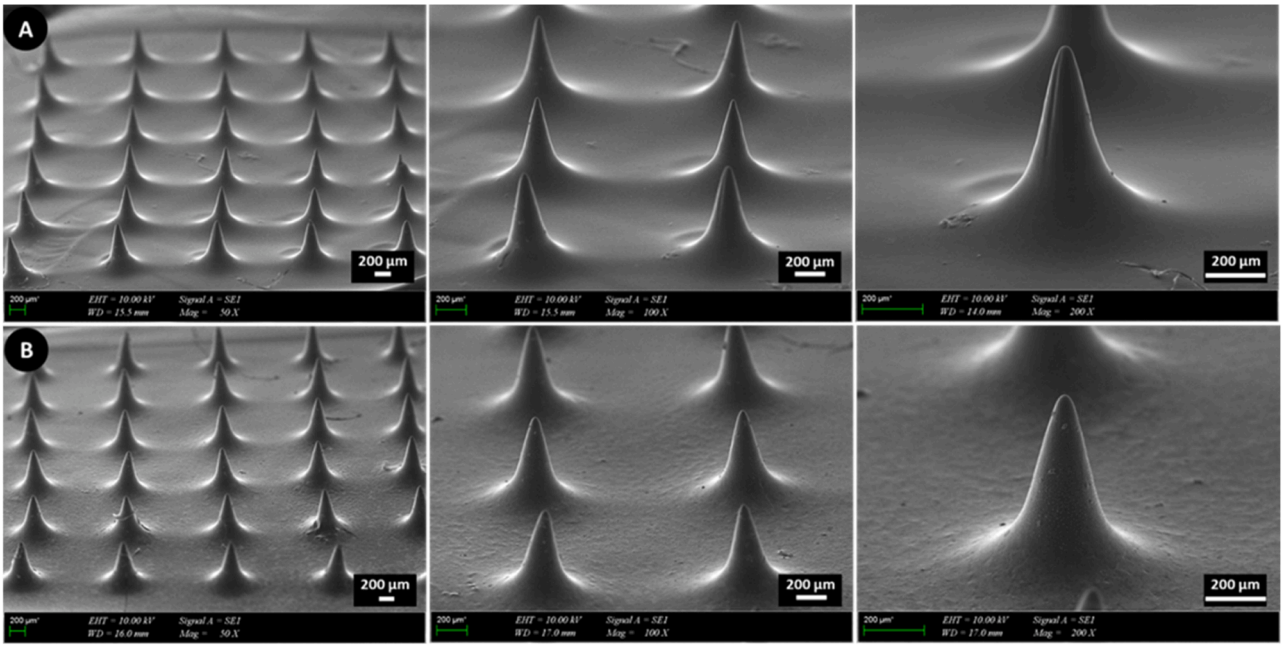

Fig. 2. SEM images of GelMA MNs (A) and AMX-loaded GelMA MNs (B).

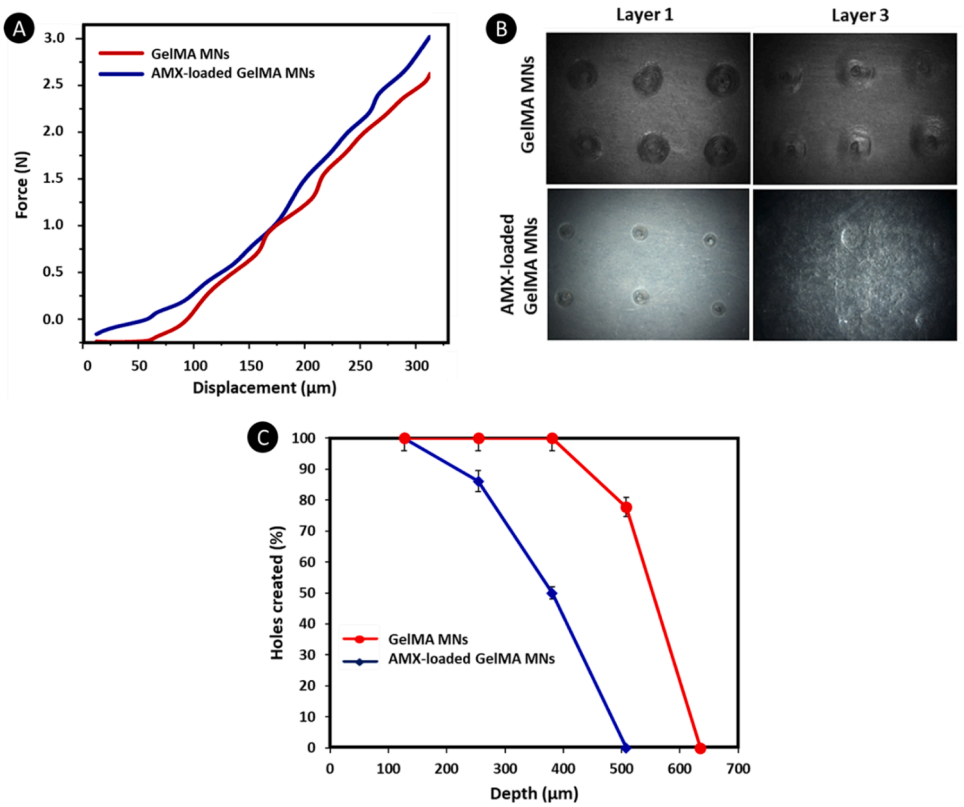

Fig. 4. (A) Force-displacement curves of GelMA MNs and AMX-loaded GelMA MNs, (B) Optical microscopy images of first and third Parafilm M® layers of GelMA MNs and AMX-loaded GelMA MNs, 5X magnification, (C) Percentage of holes created in each Parafilm M® layer following insertion of GelMA and AMX-loaded GelMA MNs.

respectively. These values are consistent with the reported 0.1 N/needle for skin puncture with MNs [51]. Moreover, according to these values, it was observed that the mechanical strength of blank GelMA MNs was relatively lower compared to AMX-loaded GelMA MNs. This is most likely because AMX interacted with polymer chains via Van der Waals interactions and strengthened the polymer network in MNs [52].

In addition to the compression test, the penetration ability of the MNs was performed. The 6×6 MN array was manually placed on the Parafilm M® layer consisting of 8 layers by thumb force. Optical microscopy images of the holes formed in the first and third sheets of the Parafilm M® layer as a result of the penetration of both GelMA MNs and AMX-loaded GelMA MNs were presented in Fig. 4B. In the placement of both types of MNs, the hole width in the layers decreased depending on the depth of placement. According to the penetration result of GelMA MNs, 4 Parafilm layers were pierced. As a result of the placement of the AMX-loaded GelMA MNs, MNs pierced 3 Parafilm layers. As shown in Fig. 4C, all needles in the GelMA MNs formed holes up to the third layer. In the fourth layer, 77.77 ± 4% of the MNs formed holes. The fourth layer agrees with the 508 μm penetration depth, where around 80% of the needle height of GelMA MNs is inserted. In the AMX-loaded GelMA MNs penetration, all needles formed holes in the first layer. 86.1 ± 3% of MNs in the second layer and 50 ± 3% in the third layer formed holes. The third layer corresponds to a penetration depth of 381 μm, where about 61% of the needle height of AMX-loaded GelMA MNs is inserted. Similar insertion profiles have been reported in previous studies [15, 53]. Moreover, the reason that GelMA MNs penetrate more deeply than AMX-loaded GelMA MNs is that the needle height of GelMA MNs (~630 μm) supported by SEM analysis is higher than that of drug-loaded MNs (~621 μm).

3.4. Swelling behaviour of GelMA MNs

The swelling ability of hydrogel MNs is critical in terms of facilitating the release of the payload and also enhancing the interaction of the MNs with the inserted cavity, stabilizing them into the punctured site [20]. To investigate their swelling behaviour, GelMA MNs and AMX-loaded GelMA MNs were immersed in PBS solution and measured their mass changes with time. The swelling ratio of MNs significantly increased within the first 1 min, as presented in Fig. 5. MNs rapidly absorbed the moisture, causing their volume to increase. Blank and AMX-loaded MNs

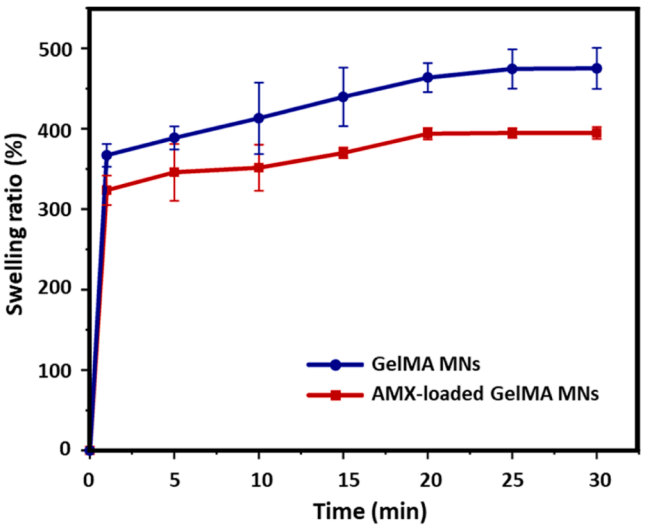

Fig. 5. Swelling ability of GelMA MNs and AMX-loaded GelMA MNs.

reached swelling equilibrium within 20 min after immersion. It is observed that the swelling ratio of blank MNs (~475%) is higher than AMX-loaded MNs (~394%). This may be due to the ionic strength increased in the swelling solution of AMX-loaded MNs. As a result, the swelling solution for AMX-loaded MNs had increased osmotic pressure, which constrained the water absorption. Similar results were reported by Wang et al [54].

3.5. In vitro drug release study

In vitro drug release tests were performed to examine the release behaviours of AMX from MNs over a 48 h period. The test was carried out in PBS (pH 7.4, 37 °C) to mimic the physiological conditions of living organisms. First, the UV spectra obtained with the concentration range of AMX from 0.2 to 1 μg/mL and a linear standard calibration curve from AMX absorption values ($R^2 = 0.998$) were created (Fig. 6A,B). The released AMX was detected by UV 201 nm absorbance. As indicated in Fig. 6C, the AMX-loaded MNs demonstrated an 80% burst release of AMX from the MNs within the first 6 h of incubation. After 48 h, all drug was released and reached 100%. The burst release may partially is caused by loosely attached drug molecules at the surface of the MNs, which are highly inclined to diffusion [55]. Also, GelMA swells by absorbing water and increases the pore size within the hydrogel matrix, ultimately facilitating the release of the loaded drug [56]. Sood et al. loaded AMX into the carboxymethyl cellulose-cl-poly(lactic acid--co-itaconic acid) hydrogel and they observed a high amount of AMX was rapidly released within the first 3 h [57].

The current studies regarding the antibiotic-loaded MNs show that the amount of the loaded drug on MNs varies from 10 μg of doxycycline [20] to 100 μg of vancomycin, in the case of MNs developed against methicillin-resistant *S. aureus* skin infections [58]. In these studies, MN production was carried out using PDMS moulds. The amount of AMX loaded into the GelMA MNs produced for this study is 5 mg, suggesting a high drug-loading capacity of GelMA MNs produced by the DLP method meaning that they would require less application frequency than other MNs.

3.6. In vitro antimicrobial activity

In this study, we have evaluated the *in vitro* antibacterial activity of AMX-loaded GelMA MNs against the Gram-positive *S. aureus* ATCC 25923 and the Gram-negative *E. coli* 25922 bacterial strains using the disc diffusion method. The growth inhibition zones around AMX-loaded GelMA MNs demonstrated the efficiency of MNs against the tested reference bacterial strains (Fig. 7A,B). The mean growth inhibition zone diameters of AMX-loaded GelMA MNs for both *S. aureus* ATCC 25923 and *E. coli* 25922 were m 22 mm and 25 mm, respectively. The hydrogel-forming MNs with antibacterial properties have been reported previously [19]. Tiraton et al. [59] fabricated sodium alginate (S)-gelatin (G) MNs patch containing clindamycin for acne treatment and found it to inhibit the growth of *Cutibacterium acnes*. In another study, a hydrogel-based wound dressing containing ciprofloxacin has been produced and shown to be effective against methicillin-resistant *S. aureus* [60]. However, the fabrication of AMX-loaded GelMA MNs with antibacterial activity against *S. aureus* and *E. coli* using the DLP 3D printing approach has not been previously reported.

4. Conclusions

In summary, a novel transdermal delivery system based on AMX-loaded GelMA MNs was successfully prepared by the DLP 3D printing technique. According to SEM analysis, sharp-tipped MNs with desired dimensions and regular morphology were obtained. Mechanical test results supported that the 3D-printed MNs showed no discontinuity or

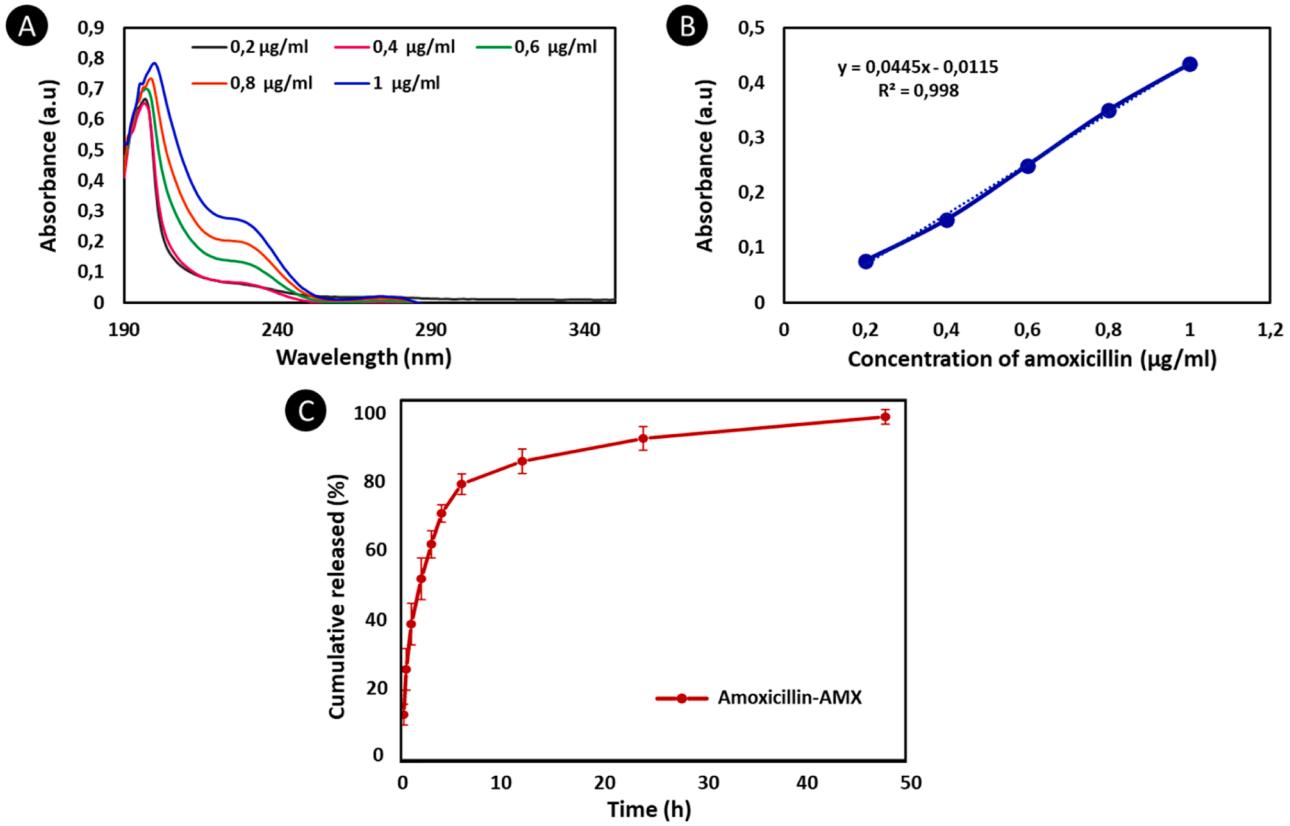

Fig. 6. *In vitro* drug release profile of AMX from the GelMA MNs: (A) Absorption spectra of AMX at different concentrations, (B) calibration curve of AMX, (C) drug release profile from the AMX-loaded GelMA MNs. All the measurements were repeated three times, and the errors were less than 5%.

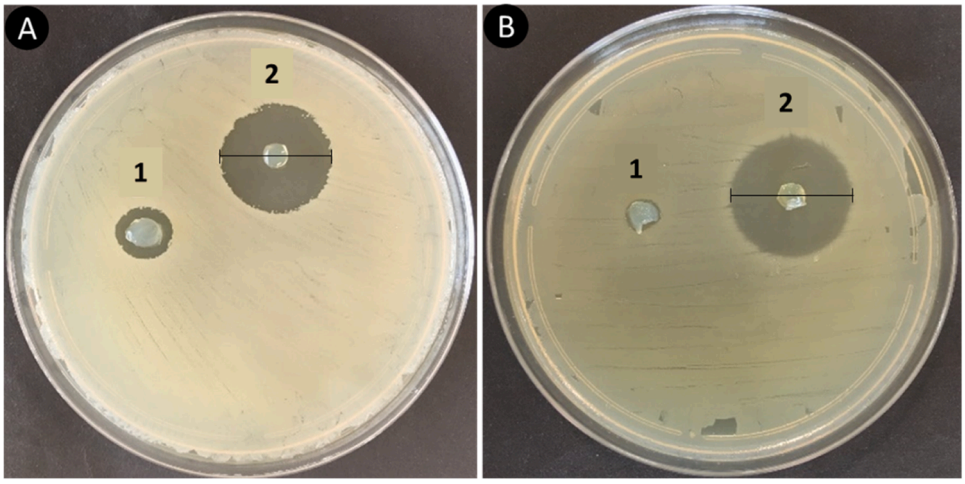

Fig. 7. Antibacterial activities of GelMA MNs: (a) against *S. aureus* 1) GelMA MNs 2) AMX-loaded GelMA MNs, (b) against *E. coli* 1) GelMA MNs 2) AMX-loaded GelMA MNs.

breakage at 300 μm displacement and were consistent with the 0.1 N/needle value suitable for transdermal applications. Moreover, 3D-printed MNs were found to rapidly release AMX within the first 6 h of incubation. In addition, the AMX-loaded GelMA MNs exhibited antibacterial activity against both Gram-positive and Gram-negative bacterial strains, suggesting their potential to be used as transdermal drug delivery devices or biomaterials such as wound dressings for tackling bacterial infections that could delay wound healing. Overall, the obtained results demonstrate that the drug-loaded MNs fabricated with the DLP printing approach can be effective for transdermal drug delivery.

Declaration of Competing Interest

The authors declare that they have no known competing financial interests or personal relationships that could have appeared to influence the work reported in this paper.

Acknowledgments

This study was supported by the Turkish Scientific and Technical Research Council (TUBITAK) 1001 Project – Tympatch. The project number is 121M670.

References

[1] Q.K. Anjani, A.D. Permana, Á. Cárcamo-Martínez, J. Domínguez-Robles, I. A. Tekko, E. Larrañeta, L.K. Vora, D. Ramadon, R.F. Donnelly, Versatility of hydrogel-forming microneedles in *in vitro* transdermal delivery of tuberculosis drugs, Eur. J. Pharm. Biopharm. 158 (2021) 294–312, https://doi.org/10.1016/j.ejpb.2020.12.003.

[2] Z. Zeng, G. Jiang, T. Liu, G. Song, Y. Sun, X. Zhang, Y. Jing, M. Feng, Y. Shi, Fabrication of gelatin methacryloyl hydrogel microneedles for transdermal delivery of metformin in diabetic rats, Bio Des. Manuf. 4 (2021) 902–911, https://doi.org/10.1007/s42242-021-00140-9.

[3] X. Zhou, Z. Luo, A. Baidya, H. Kim, C. Wang, X. Jiang, M. Qu, J. Zhu, L. Ren, F. Vajhadin, P. Tebon, N. Zhang, Y. Xue, Y. Feng, C. Xue, Y. Chen, K. Lee, J. Lee, S. Zhang, C. Xu, N. Ashammakhi, S. Ahadian, M.R. Dokmeci, Z. Gu, W. Sun, A. Khademhosseini, Biodegradable β-cyclodextrin conjugated gelatin methacryloyl microneedle for delivery of water-insoluble drug, Adv. Healthc. Mater. 9 (2020), 2000527, https://doi.org/10.1002/adhm.202000527.

[4] A.A. Seetharam, H. Choudhry, M.A. Bakhrebah, W.H. Abdulaal, M.S. Gupta, S.M. D. Rizvi, Q. Alam, D.V.Gowda Siddaramaiah, A. Moin, Microneedles drug delivery systems for treatment of cancer: a recent update, Pharmaceutics 12 (2020) 1–27, https://doi.org/10.3390/pharmaceutics12111101.

[5] M. Dalvi, P. Kharat, P. Thakor, V. Bhavana, S.B. Singh, N.K. Mehra, Panorama of dissolving microneedles for transdermal drug delivery, Life Sci. 284 (2021), 119877, https://doi.org/10.1016/j.lfs.2021.119877.

[6] T. Liu, G. Luo, M. Xing, Biomedical applications of polymeric microneedles for transdermal therapeutic delivery and diagnosis: current status and future perspectives, Adv. Ther. 3 (2020), 1900140, https://doi.org/10.1002/ADTP.201900140.

[7] T. Waghule, G. Singhvi, S.K. Dubey, M.M. Pandey, G. Gupta, M. Singh, K. Dua, Microneedles: a smart approach and increasing potential for transdermal drug delivery system, Biomed. Pharmacother. 109 (2019) 1249–1258, https://doi.org/10.1016/j.biopha.2018.10.078.

[8] K. Ita, Dissolving microneedles for transdermal drug delivery: advances and challenges, Biomed. Pharmacother. 93 (2017) 1116–1127, https://doi.org/10.1016/j.biopha.2017.07.019.

[9] E. McAlister, B. Dutton, L.K. Vora, L. Zhao, A. Ripolin, D.S.Z.B.P.H. Zahari, H. L. Quinn, I.A. Tekko, A.J. Courtenay, S.A. Kelly, A.M. Rodgers, L. Steiner, G. Levin, E. Levy-Nissenbaum, N. Shterman, H.O. McCarthy, R.F. Donnelly, Directly compressed tablets: a novel drug-containing reservoir combined with hydrogel-forming microneedle arrays for transdermal drug delivery, Adv. Healthc. Mater. 10 (2021), 2001256, https://doi.org/10.1002/adhm.202001256.

[10] F. Meng, A. Hasan, M. Mahdi Nejadi Babadaei, P. Hashemi Kani, A. Jouya Talaei, M. Sharifi, T. Cai, M. Falahati, Y. Cai, Polymeric-based microneedle arrays as potential platforms in the development of drugs delivery systems, J. Adv. Res. 26 (2020) 137–147, https://doi.org/10.1016/j.jare.2020.07.017.

[11] M.R. Prausnitz, Downloaded from www.annualreviews.org access provided by Auckland university of technology on 01/28/19. for personal use only, Annu. Rev. Chem. Biomol. Eng. 8 (2017) 177–200.

[12] V. Alimardani, S.S. Abolmaali, A.M. Tamaddon, M. Ashfaq, Recent advances on microneedle arrays-mediated technology in cancer diagnosis and therapy, Drug Deliv. Transl. Res. 11 (2021) 788–816, https://doi.org/10.1007/s13346-020-00819-z.

[13] S.N. Economidou, D. Douroumis, 3D printing as a transformative tool for microneedle systems: recent advances, manufacturing considerations and market potential, Adv. Drug Deliv. Rev. 173 (2021) 60–69, https://doi.org/10.1016/j.addr.2021.03.007.

[14] W. Yao, D. Li, Y. Zhao, Z. Zhan, G. Jin, H. Liang, R. Yang, 3D Printed multi-functional hydrogel microneedles based on high-precision digital light processing, Micromachines 11 (2020) 17, https://doi.org/10.3390/mi11010017.

[15] D.F.S. Fonseca, P.C. Costa, I.F. Almeida, P. Dias-Pereira, I. Correia-Sá, V. Bastos, H. Oliveira, C. Vilela, A.J.D. Silvestre, C.S.R. Freire, Swellable gelatin methacryloyl microneedles for extraction of interstitial skin fluid toward minimally invasive monitoring of urea, Macromol. Biosci. 20 (2020) 1–11, https://doi.org/10.1002/mabi.202000195.

[16] B.Z. Chen, M. Ashfaq, D.D. Zhu, X.P. Zhang, X.D. Guo, Controlled delivery of insulin using rapidly separating microneedles fabricated from genipin-crosslinked gelatin, Macromol. Rapid Commun. 39 (2018), 1800075, https://doi.org/10.1002/marc.201800075.

[17] M. Sirbubalo, A. Tucak, K. Muhamedagic, L. Hindija, O. Rahić, J. Hadžiabdić, A. Cekic, D. Begic-Hajdarevic, M.C. Husic, A. Dervišević, E. Vranić, 3D printing—a "touch-button" approach to manufacture microneedles for transdermal drug delivery, Pharmaceutics 13 (2021) 924, https://doi.org/10.3390/pharmaceutics13070924.

[18] E. Larrañeta, S. Stewart, M. Ervine, R. Al-Kasasbeh, R.F. Donnelly, Hydrogels for hydrophobic drug delivery. classification, synthesis and applications, J. Funct. Biomater. 9 (2018) 13, https://doi.org/10.3390/jfb9010013.

[19] J.G. Turner, L.R. White, P. Estrela, H.S. Leese, Hydrogel-forming microneedles: current advancements and future trends, Macromol. Biosci. 21 (2021), 2000307, https://doi.org/10.1002/mabi.202000307.

[20] Z. Luo, W. Sun, J. Fang, K.J. Lee, S. Li, Z. Gu, M.R. Dokmeci, A. Khademhosseini, Biodegradable gelatin methacryloyl microneedles for transdermal drug delivery, Adv. Healthc. Mater. 8 (2019) 1–9, https://doi.org/10.1002/adhm.201801054.

[21] A. Ullah, M. Jang, H. Khan, H.J. Choi, S. An, D. Kim, Y.R. Kim, U.K. Kim, G.M. Kim, Microneedle array with a pH-responsive polymer coating and its application in smart drug delivery for wound healing, Sens. Actuators B Chem. 345 (2021), 130441, https://doi.org/10.1016/j.snb.2021.130441.

[22] J.W. Nichol, S.T. Koshy, H. Bae, C.M. Hwang, S. Yamanlar, A. Khademhosseini, Cell-laden microengineered gelatin methacrylate hydrogels, Biomaterials 31 (2010) 5536–5544, https://doi.org/10.1016/j.biomaterials.2010.03.064.
[23] K. Rahali, G. Ben Messaoud, C.J.F. Kahn, L. Sanchez-Gonzalez, M. Kaci, F. Cleymand, S. Fleutot, M. Linder, S. Desobry, E. Arab-Tehrany, Synthesis and characterization of nanofunctionalized gelatin methacrylate hydrogels, Int. J. Mol. Sci. 18 (2017) 2675, https://doi.org/10.3390/ijms18122675.
[24] S. Xiao, T. Zhao, J. Wang, C. Wang, J. Du, L. Ying, J. Lin, C. Zhang, W. Hu, L. Wang, K. Xu, Gelatin Methacrylate, GelMA)-Based hydrogels for cell transplantation: an effective strategy for tissue engineering, Stem Cell Rev. Rep. 15 (2019) 664–679, https://doi.org/10.1007/s12015-019-09893-4.
[25] F.K. Aldawood, A. Andar, S. Desai, A comprehensive review of microneedles: types, materials, processes, characterizations and applications, Polymers 13 (2021) 1–34, https://doi.org/10.3390/polym13162815 (Basel).
[26] X. Jin, D.D. Zhu, B.Z. Chen, M. Ashfaq, X.D. Guo, Insulin delivery systems combined with microneedle technology, Adv. Drug Deliv. Rev. 127 (2018) 119–137, https://doi.org/10.1016/j.addr.2018.03.011.
[27] A.R. Johnson, A.T. Procopio, Low cost additive manufacturing of microneedle masters, 3D Print. Med. 5 (2019) 2, https://doi.org/10.1186/s41205-019-0039-x.
[28] I. Xenikakis, K. Tsongas, E.K. Tzimtzimis, C.K. Zacharis, N. Theodoroula, E. P. Kalogianni, E. Demiri, I.S. Vizirianakis, D. Tzetzis, D.G. Fatouros, Fabrication of hollow microneedles using liquid crystal display (LCD) vat polymerization 3D printing technology for transdermal macromolecular delivery, Int. J. Pharm. 597 (2021), 120303, https://doi.org/10.1016/j.ijpharm.2021.120303.
[29] Y. Zeng, Y. Yan, H. Yan, C. Liu, P. Li, P. Dong, Y. Zhao, J. Chen, 3D printing of hydroxyapatite scaffolds with good mechanical and biocompatible properties by digital light processing, J. Mater. Sci. 53 (2018) 6291–6301, https://doi.org/10.1007/s10853-018-1992-2.
[30] S.R. Dabbagh, M.R. Sarabi, R. Rahbarghazi, E. Sokullu, A.K. Yetisen, S. Tasoglu, 3D-printed microneedles in biomedical applications, IScience 24 (2021), 102012, https://doi.org/10.1016/J.ISCI.2020.102012.
[31] D. Shin, J. Hyun, Silk fibroin microneedles fabricated by digital light processing 3D printing, J. Ind. Eng. Chem. 95 (2021) 126–133, https://doi.org/10.1016/j.jiec.2020.12.011.
[32] W. Zhu, X. Ma, M. Gou, D. Mei, K. Zhang, S. Chen, 3D printing of functional biomaterials for tissue engineering, Curr. Opin. Biotechnol. 40 (2016) 103–112, https://doi.org/10.1016/j.copbio.2016.03.014.
[33] P.N. Bernal, P. Delrot, D. Loterie, Y. Li, J. Malda, C. Moser, R. Levato, Volumetric bioprinting of complex living-tissue constructs within seconds, Adv. Mater. 31 (2019), 1904209, https://doi.org/10.1002/adma.201904209.
[34] Y. Lu, S.N. Mantha, D.C. Crowder, S. Chinchilla, K.N. Shah, Y.H. Yun, R.B. Wicker, J.-W. Choi, Microstereolithography and characterization of poly(propylene fumarate)-based drug-loaded microneedle arrays, Biofabrication 7 (2015) 45001, https://doi.org/10.1088/1758-5090/7/4/045001.
[35] Q. Yang, W. Zhong, L. Xu, H. Li, Q. Yan, Y. She, G. Yang, Recent progress of 3D-printed microneedles for transdermal drug delivery, Int. J. Pharm. 593 (2021), 120106, https://doi.org/10.1016/J.IJPHARM.2020.120106.
[36] Q. Hu, R. Lu, S. Liu, Y. Liu, Y. Gu, H. Zhang, 3D printing GelMA/PVA interpenetrating polymer networks scaffolds mediated with CuO nanoparticles for angiogenesis, Macromol. Biosci. (2022), https://doi.org/10.1002/mabi.202200208.
[37] S.D. Gittard, P.R. Miller, C. Jin, T.N. Martin, R.D. Boehm, B.J. Chisholm, S. J. Stafslien, J.W. Daniels, N. Cilz, N.A. Monteiro-Riviere, A. Nasir, R.J. Narayan, Deposition of antimicrobial coatings on microstereolithography-fabricated microneedles, JOM 63 (2011) 59–68, https://doi.org/10.1007/s11837-011-0093-3.
[38] H. Shirahama, B.H. Lee, L.P. Tan, N.J. Cho, Precise tuning of facile one-pot gelatin methacryloyl (GelMA) synthesis, Sci. Rep. 6 (2016) 31036, https://doi.org/10.1038/srep31036.
[39] E. Larrañeta, J. Moore, E.M. Vicente-Pérez, P. González-Vázquez, R. Lutton, A. D. Woolfson, R.F. Donnelly, A proposed model membrane and test method for microneedle insertion studies, Int. J. Pharm. 472 (2014) 65–73, https://doi.org/10.1016/j.ijpharm.2014.05.042.
[40] J. Zhu, X. Zhou, H.J. Kim, M. Qu, X. Jiang, K.J. Lee, L. Ren, Q. Wu, C. Wang, X. Zhu, P. Tebon, S. Zhang, J. Lee, N. Ashammakhi, S. Ahadian, M.R. Dokmeci, Z. Gu, W. Sun, A. Khademhosseini, Gelatin methacryloyl microneedle patches for minimally invasive extraction of skin interstitial fluid, Small 16 (2020) 1–9, https://doi.org/10.1002/smll.201905910.
[41] K.J. Krieger, N. Bertollo, M. Dangol, J.T. Sheridan, M.M. Lowery, E. D. O'Cearbhaill, Simple and customizable method for fabrication of high-aspect ratio microneedle molds using low-cost 3D printing, Microsyst. Nanoeng. 5 (2019) 42, https://doi.org/10.1038/s41378-019-0088-8.
[42] S. Mirzaeei, M. Mansurian, K. Asare-Addo, A. Nokhodchi, Metronidazole-and amoxicillin-loaded plga and pcl nanofibers as potential drug delivery systems for the treatment of periodontitis: *in vitro* and *in vivo* evaluations, Biomedicines 9 (2021) 975, https://doi.org/10.3390/biomedicines9080975.
[43] S. Wang, F. Zheng, Y. Huang, Y. Fang, M. Shen, M. Zhu, X. Shi, Encapsulation of amoxicillin within laponite-doped poly(lactic-co-glycolic acid) nanofibers: Preparation, characterization, and antibacterial activity, ACS Appl. Mater. Interfaces 4 (2012) 6393–6401, https://doi.org/10.1021/am302130b.
[44] F. Zheng, S. Wang, S. Wen, M. Shen, M. Zhu, X. Shi, Characterization and antibacterial activity of amoxicillin-loaded electrospun nano-hydroxyapatite/poly (lactic-co-glycolic acid) composite nanofibers, Biomaterials 34 (2013) 1402–1412, https://doi.org/10.1016/j.biomaterials.2012.10.071.
[45] K. Irem Deniz, S. Ulag, O. Gunduz, Investigation of the properties of encapsulated hydrophilic and hydrophobic drugs in whey protein microparticles, Mater. Lett. 324 (2022), 132664, https://doi.org/10.1016/j.matlet.2022.132664.
[46] F. Nazir, I. Ashraf, M. Iqbal, T. Ahmad, S. Anjum, 6-deoxy-aminocellulose derivatives embedded soft gelatin methacryloyl (GelMA) hydrogels for improved wound healing applications: *in vitro* and *in vivo* studies, Int. J. Biol. Macromol. 185 (2021) 419–433, https://doi.org/10.1016/j.ijbiomac.2021.06.112.
[47] K. Rahimi Mamaghani, S. Morteza Naghib, A. Zahedi, M. Mozafari, Synthesis and microstructural characterization of GelMa/PEGDA hybrid hydrogel containing graphene oxide for biomedical purposes, Mater. Today Proc. 5 (2018) 15635–15644, https://doi.org/10.1016/j.matpr.2018.04.173.
[48] S. Sreekumaran, A. Radhakrishnan, A.A. Rauf, G.M. Kurup, Nanohydroxyapatite incorporated photocrosslinked gelatin methacryloyl/poly(ethylene glycol) diacrylate hydrogel for bone tissue engineering, Prog. Biomater. 10 (2021) 43–51, https://doi.org/10.1007/s40204-021-00150-x.
[49] W. Li, R.N. Terry, J. Tang, M.R. Feng, S.P. Schwendeman, M.R. Prausnitz, Rapidly separable microneedle patch for the sustained release of a contraceptive, Nat. Biomed. Eng. 3 (2019) 220–229, https://doi.org/10.1038/s41551-018-0337-4.
[50] Q.L. Wang, J.W. Ren, B.Z. Chen, X. Jin, C.Y. Zhang, X.D. Guo, Effect of humidity on mechanical properties of dissolving microneedles for transdermal drug delivery, J. Ind. Eng. Chem. 59 (2018) 251–258, https://doi.org/10.1016/j.jiec.2017.10.030.
[51] D.D. Zhu, B.Z. Chen, M.C. He, X.D. Guo, Structural optimization of rapidly separating microneedles for efficient drug delivery, J. Ind. Eng. Chem. 51 (2017) 178–184, https://doi.org/10.1016/j.jiec.2017.02.030.
[52] M.R. Zare, M. Khorram, S. Barzegar, B. Sarkari, Q. Asgari, S. Ahadian, K. Zomorodian, Dissolvable carboxymethyl cellulose/polyvinylpyrrolidone microneedle arrays for transdermal delivery of Amphotericin B to treat cutaneous leishmaniasis, Int. J. Biol. Macromol. 182 (2021) 1310–1321, https://doi.org/10.1016/j.ijbiomac.2021.05.075.
[53] L.K. Vora, R.F. Donnelly, E. Larrañeta, P. González-Vázquez, R.R.S. Thakur, P. R. Vavia, Novel bilayer dissolving microneedle arrays with concentrated PLGA nano-microparticles for targeted intradermal delivery: proof of concept, J. Control. Release 265 (2017) 93–101, https://doi.org/10.1016/j.jconrel.2017.10.005.
[54] T.-L. Wang, Z. Zhou, J.-F. Liu, X.-D. Hou, Z. Zhou, Y.-L. Dai, Z. Hou, F. Chen, L.-P. Zheng, Donut-like MOFs of copper/nicotinic acid and composite hydrogels with superior bioactivity for rh-bFGF delivering and skin wound healing, J. Nanobiotechnol. 19 (2021) 275, https://doi.org/10.1186/s12951-021-01014-z.
[55] M. Vigata, C. Meinert, S. Pahoff, N. Bock, D.W. Hutmacher, Gelatin methacryloyl hydrogels control the localized delivery of albumin-bound paclitaxel, Polymers 12 (2020) 501, https://doi.org/10.3390/polym12020501 (Basel).
[56] G. Zidan, C.A. Greene, A. Etxabide, I.D. Rupenthal, A. Seyfoddin, Gelatine-based drug-eluting bandage contact lenses: effect of PEGDA concentration and manufacturing technique, Int. J. Pharm. 599 (2021), 120452, https://doi.org/10.1016/j.ijpharm.2021.120452.
[57] S. Sood, V.K. Gupta, S. Agarwal, K. Dev, D. Pathania, Controlled release of antibiotic amoxicillin drug using carboxymethyl cellulose-cl-poly(lactic acid-co-itaconic acid) hydrogel, Int. J. Biol. Macromol. 101 (2017) 612–620, https://doi.org/10.1016/j.ijbiomac.2017.03.103.
[58] J. Ziesmer, P. Tajpara, N.J. Hempel, M. Ehrström, K. Melican, L. Eidsmo, G. A. Sotiriou, Vancomycin-loaded microneedle arrays against methicillin-resistant staphylococcus aureus skin infections, Adv. Mater. Technol. 6 (2021), https://doi.org/10.1002/admt.202001307.
[59] T. Tiraton, O. Suwantong, P. Chuysinuan, P. Ekabutr, P. Niamlang, T. Khampieng, P. Supaphol, Biodegradable microneedle fabricated from sodium alginate-gelatin for transdermal delivery of clindamycin, Mater. Today Commun. 32 (2022), 104158, https://doi.org/10.1016/j.mtcomm.2022.104158.
[60] Y. Shi, V.X. Truong, K. Kulkarni, Y. Qu, G.P. Simon, R.L. Boyd, P. Perlmutter, T. Lithgow, J.S. Forsythe, Light-triggered release of ciprofloxacin from an in situ forming click hydrogel for antibacterial wound dressings, J. Mater. Chem. B 3 (2015) 8771–8774, https://doi.org/10.1039/c5tb01820j.